

VIP Very Important Paper

Heteroaromatic Inhibitors of the Astacin Proteinases Meprin α , Meprin β and Ovastacin Discovered by a Scaffold-Hopping ApproachKathrin Tan,^[a] Christian Jäger,^[a, b] Hagen Körschgen,^[c] Stefanie Geissler,^[a] Dagmar Schlenzig,^[a] Mirko Buchholz,^[a] Walter Stöcker,^[c] and Daniel Ramsbeck^{*[a]}

Astacin metalloproteinases, in particular meprins α and β , as well as ovastacin, are emerging drug targets. Drug-discovery efforts have led to the development of the first potent and selective inhibitors in the last few years. However, the most recent compounds are based on a highly flexible tertiary amine scaffold that could cause metabolic liabilities or decreased potency due to the entropic penalty upon binding to the target. Thus, the aim of this study was to discover novel conformation-

ally constrained scaffolds as starting points for further inhibitor optimization. Shifting from flexible tertiary amines to rigid heteroaromatic cores resulted in a boost in inhibitory activity. Moreover, some compounds already exhibited higher activity against individual astacin proteinases compared to recently reported inhibitors and also a favorable off-target selectivity profile, thus qualifying them as very suitable chemical probes for target validation.

Introduction

Proteinases of the astacin family as potential drug targets recently moved into the focus of drug development. In humans, this family comprises the meprins α and β , ovastacin and BMP-1.^[1] The last, together with its variants, that is, tolloids, have been in the focus of drug development for the last two decades as targets for the development of antifibrotic drugs.^[2] In contrast, the remaining human astacins only emerged as drug targets recently. Due to their procollagenase activity, meprin α and β are involved in the assembly of collagen fibrils like BMP-1 and are also potentially involved in fibrotic disorders, such as keloids or lung fibrosis.^[3] Furthermore, they have been linked to cancer^[4] and kidney injury^[5], as they are able to cleave several components of the extracellular matrix and thus contribute to ECM remodeling. Hence, meprins could promote the migration and invasion of cancer cells into healthy tissue or contribute to the damage of renal tissue. In particular meprin β is involved in

the proteolytic processing of several cytokines and was also discussed as a potential drug target for inflammatory bowel disease.^[6] Furthermore, meprin β is able to cleave the amyloid precursor protein, resulting in the release of neurotoxic amyloid β peptides. Hence, it was revealed as an alternative β -secretase in Alzheimer's disease.^[7] Ovastacin was found to be involved in the regulation of female fertility.^[8] Small amounts of ovastacin seeping out of the oocytes lead to premature hardening of the zona pellucida, which is physiologically controlled by the endogenous inhibitor fetuin-B.^[9] Fetuin deficiency causes zona pellucida hardening, thus preventing sperm cells from entering the oocyte and consequently leading to infertility. Hence, inhibition of ovastacin by small molecules *in vivo* could be a novel approach addressing female infertility or a novel supplement to facilitate *in vitro* fertilization. Moreover, ovastacin was also found to be expressed by several types of tumors as tumor-oocyte-neoantigen.^[10] A potential involvement in tumor migration and invasion is currently under investigation and might render ovastacin as anticancer target in the future.

Recently, we reported the development of selective meprin β inhibitors starting from the broad-spectrum metalloproteinase inhibitor NNGH.^[11] Further structural modification and simplification of the sulfonamide backbone by $\text{SO}_2 \rightarrow \text{CH}_2$ switching led to a tertiary amine hydroxamate scaffold. This modification significantly improved the inhibitor selectivity against off-target metalloproteinases, that is, MMPs and ADAMs. The derivatization of this scaffold revealed potent and selective inhibitors of either meprin α or β .^[12,13] More recently, selected compounds of this chemotype were also found to be potent inhibitors of ovastacin (Figure 1), rendering them as pan-selective astacin inhibitors.^[14] Nevertheless, the tertiary amine motif exhibits a high conformational freedom, potentially leading to entropic penalty upon binding to the active site of the enzyme. Furthermore, the benzylic $\text{CH}_2\text{-N}$ bonds represent hotspots that might lead to reduced metabolic stability due to oxidative

[a] K. Tan, C. Jäger, Dr. S. Geissler, Dr. D. Schlenzig, Dr. M. Buchholz, Dr. D. Ramsbeck
Department of Drug Design and Target Validation MWT
Fraunhofer Institute for Cell Therapy and Immunology IZI
Biocenter, Weinbergweg 22, 06120 Halle (Saale) (Germany)
E-mail: daniel.ramsbeck@izi.fraunhofer.de

[b] C. Jäger
present address: Vivoryon Therapeutics N.V.,
Weinbergweg 22, 06120 Halle (Saale) (Germany)

[c] Dr. H. Körschgen, Prof. Dr. W. Stöcker
Institute of Molecular Physiology, Cell and Matrix Biology
Johannes Gutenberg-University Mainz
Johann-Joachim-Becher-Weg 7, 55128 Mainz (Germany)

Supporting information for this article is available on the WWW under <https://doi.org/10.1002/cmdc.202000822>

© 2020 The Authors. ChemMedChem published by Wiley-VCH GmbH. This is an open access article under the terms of the Creative Commons Attribution Non-Commercial NoDerivs License, which permits use and distribution in any medium, provided the original work is properly cited, the use is non-commercial and no modifications or adaptations are made.

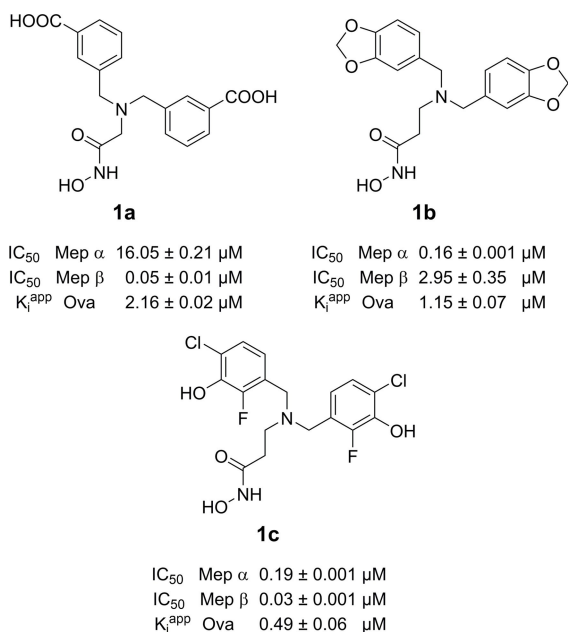


Figure 1. Tertiary amine-based inhibitors of meprin α/β and ovastacin with different selectivity profiles.

dealkylation, albeit the compounds exhibited acceptable plasma half-lives in rats.^[12] However, these putative shortcomings of the tertiary amines prompted us to investigate possible replacements to generate bioisosteric scaffolds suitable for the development of novel astacin inhibitors.

Results and Discussion

Scaffold design

As mentioned above, the tertiary amine based compounds exhibit a high degree of conformational freedom, due to the high flexibility of the aliphatic amine and a high number of rotatable bonds. Hence, this flexibility might lead to entropic penalty, caused by the loss of rotational freedom upon binding to the target. A general strategy to overcome this issue in lead optimization is the structural preorganization or rigidification of a scaffold, for example by cyclization or macrocyclization of the respective compounds. Hence, we assumed that the replacement of the central tertiary amine by a suitable heterocycle could lead to more rigid compounds and potentially improve binding of the inhibitors to meprin α and β and maybe also other astacin proteinases, for example, ovastacin. However, initial experiments that replaced the acyclic tertiary amine **1** by an alicyclic amine, i.e., a pyrrolidine moiety, just led to equipotent inhibitors without any improved activity towards meprin α or β (not shown). Thus, we next focused on heteroaromatic cores as potential isosteres of the tertiary amine, concurrently also causing deeper changes in chemical- and physicochemical properties, that is, a scaffold hopping,

rather than a simple aliphatic cyclization of the amine and a locked conformation (Figure 2).

We formally assumed three possible heteroaromatic cyclizations for the rigidification of the tertiary amine, a "1,2,3" and "1,2,4" cyclization yielding scaffolds **2** and **3**, or a ring fusion yielding scaffold **4**, respectively. As either glycine and β -alanine derivatives were found to be suitable spacers between the tertiary amine and the hydroxamic acid and could affect the inhibitor activity against meprin α or β and ovastacin,^[12–14] both spacers between hydroxamic acid and the heteroaromatic cores were investigated, as well. Prototypic, synthetically tractable inhibitors of these three scaffolds are represented by 2,5-diphenyl-1-yl-pyrroles **2a, b**, 3,5-diphenyl-1-yl-pyrazoles **3a, b** and 2-phenyl-1-yl-indoles **4a, b**.

To investigate if these compounds could potentially be able to mimic the bioactive conformation of the tertiary amine scaffold, we utilized a flexible alignment approach. Recently, the structure of meprin β in complex with compound **1a** was elucidated (internal communication). Thus, we intended to use the conformation of the inhibitor bound to the active site of meprin β as fixed template for the flexible alignment of the scaffold prototypes.

However, the crystal structure of meprin β in complex with compound **1a** and further molecular dynamics simulations revealed a high flexibility of one of the two benzylic residues. While the moiety addressing the S_1' pocket and the hydroxamic acid were quite fixed in these complexes, the benzyl residue targeting the S_1 pocket, that is, R^{184} , exhibited a high degree of flexibility. This is also true for R^{184} itself, rendering the S_1 pocket of meprin β rather flexible. Hence, we only fixed the respective substructures in the template for the flexible alignments, i.e. the hydroxamic acid and the benzyl moiety addressing S_1' , while the second benzyl residue was allowed to be flexible

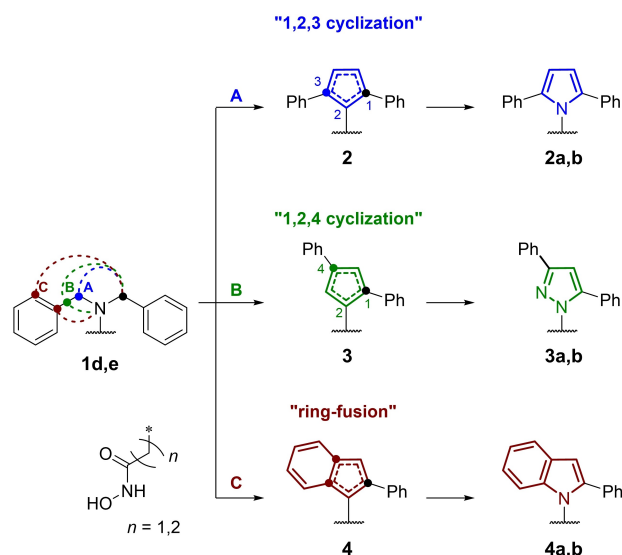


Figure 2. Possible strategies for rigidification of the tertiary amine scaffold: A) "1,2,3" cyclization leading to prototypic pyrroles **2a, b**; B) "1,2,4"-cyclization leading to prototypic pyrazoles **3a, b**; C) "ring-fusion" leading to prototypic indoles **4a, b** as potential novel inhibitors of astacin proteinases.

during the simulations (Figure 3A and B). This setup provided alignment results with reasonable conformations and geometries of the respective central heteroaromatic cores (Figure 3C–H). Although all compounds match the hydroxamic acid and the benzyl moiety addressing the S_1' pocket due to the fixed template, no complete match of the second benzyl residue of the actual starting conformation of the template, that is, the conformation of enzyme bound ligand **1a**, could be observed, regardless of the spacer between heterocycle and hydroxamic acid. Nevertheless, the alignments of the pyrrole (**2a, b**, Figure 3C and F) and indole derivatives (**4a, b**, Figure 3E and H) suggested a better conformational fit of the compounds compared to the tertiary amine template, as the respective pyrazole-derivatives (**3a, b**, Figure 3D and G), indicating a more suitable replacement of the amine scaffold. Based on this, we assumed that compounds **2a** and **b** as well as **4a** and **b** could be putative novel astacin inhibitors based on hitherto unexplored scaffolds in the context of metzincin proteinases.

To further corroborate these findings, in particular integrating also the environment of the target proteins, docking studies were performed. For this purpose, a constraint was used, tethering the hydroxamic acid substructure to ensure a proper placement and zinc-binding of the ligands within the active site cleft of the receptor proteins. The resulting docking solutions revealed poses for all compounds within the active site cleft of meprin β that are slightly diverging from the X-ray conformation of **1a** (Figure 4). Although lacking functional groups, i.e., carboxylates, may rule out attractive interactions with R^{184} and R^{238} , thus leading to a different orientation of the scaffold within the active site cleft. For the compounds with C_1 spacer between

heteroaromatic core and hydroxamic acid, that is, **2a**, and **4a** (Figure 4A, G), the aryl moiety addressing the S_1 site is in a quite similar orientation like for **1a**, suggesting the possibility of the formation of interactions with R^{184} upon suitable functionalization and decoration. However, the docking solutions for the pyrazole derivative **3a** suggest no interaction with the S_1 residue (Figure 4D). On the other hand, the moiety addressing the S_1' pocket is shifted deeper into the subpocket compared to **1a**. While for **3a** (Figure 4D) the deviation from the conformation of **1a** is marginal, the aryl moiety of **2a** (Figure 4A) and **4a** (Figure 4G) is moved deeper in the S_1' pocket and thus closer to R^{238} compared to **1a**.

However, the docking solutions of **2a** and **4a** suggest possible interactions with Y^{211} at the bottom of the active site cleft and also F^{216} shaping the lower rim of the cleft of meprin β . The docking solutions of **2a**, **3a** and **4a** within the active site of meprin α exhibit a slightly different orientation compared to the poses found for meprin β (Figure 4B, E, H). This might be due to a more narrow active site cleft in the homology model of meprin α , created by the bulky Y^{187} shaping the S_1 subpocket. However, this could enable possible π – π interactions of Y^{187} and the aryl residue or even the heteroaromatic cores of **2a**, **3a** and **4a**, respectively, while the second aryl-moiety addresses the S_1' subpocket.

The docking solutions of the compounds within the active site of ovastacin also suggest potential π – π interactions of the heteroaromatic cores, although with F^{243} , rather than the residue shaping the S_1 pocket, that is, F^{214} (Figure 4C, F, I). Like for the meprins, the docking poses also revealed a proper positioning of the putative inhibitors within the S_1' pocket.

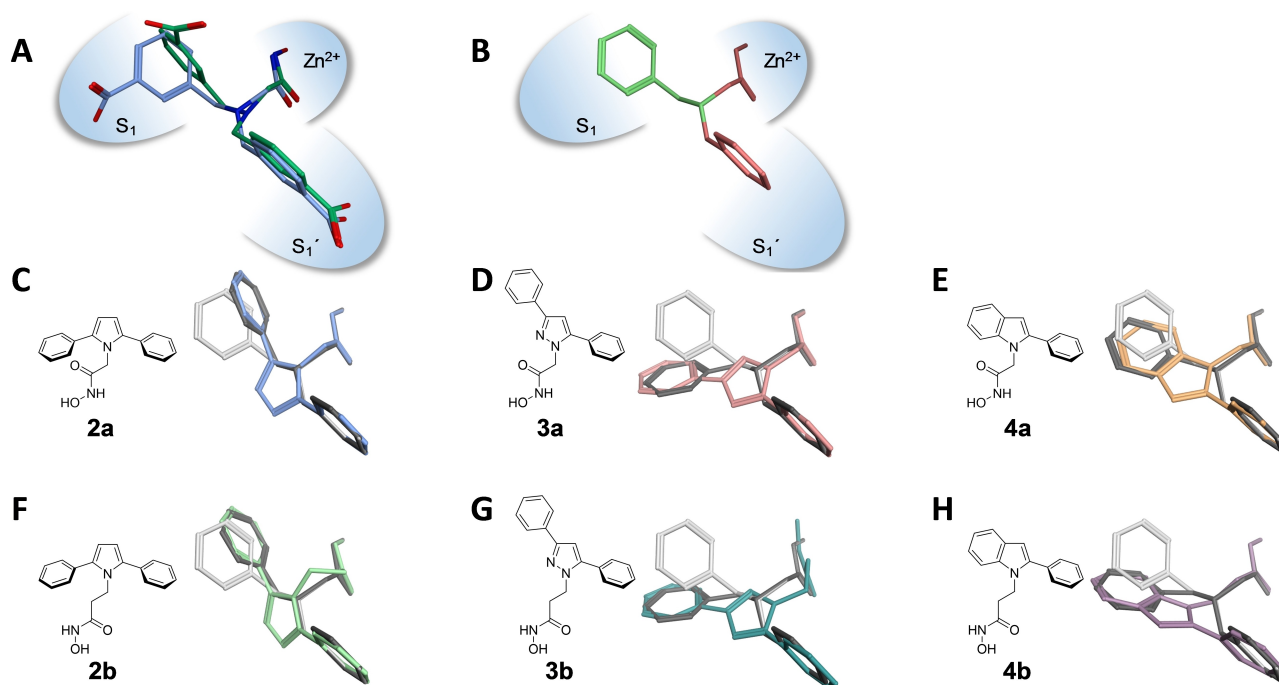


Figure 3. Flexible alignments of putative novel inhibitors. A) Conformations of **1a** from meprin β co-crystal; B) template for flexible alignment derived from (A), red – fixed atoms, green – free atoms; C–H) flexible alignments of compounds **2a, b, 3a, b, 4a, b** (coloured), template start conformation (light grey), template aligned with individual compounds (dark grey).

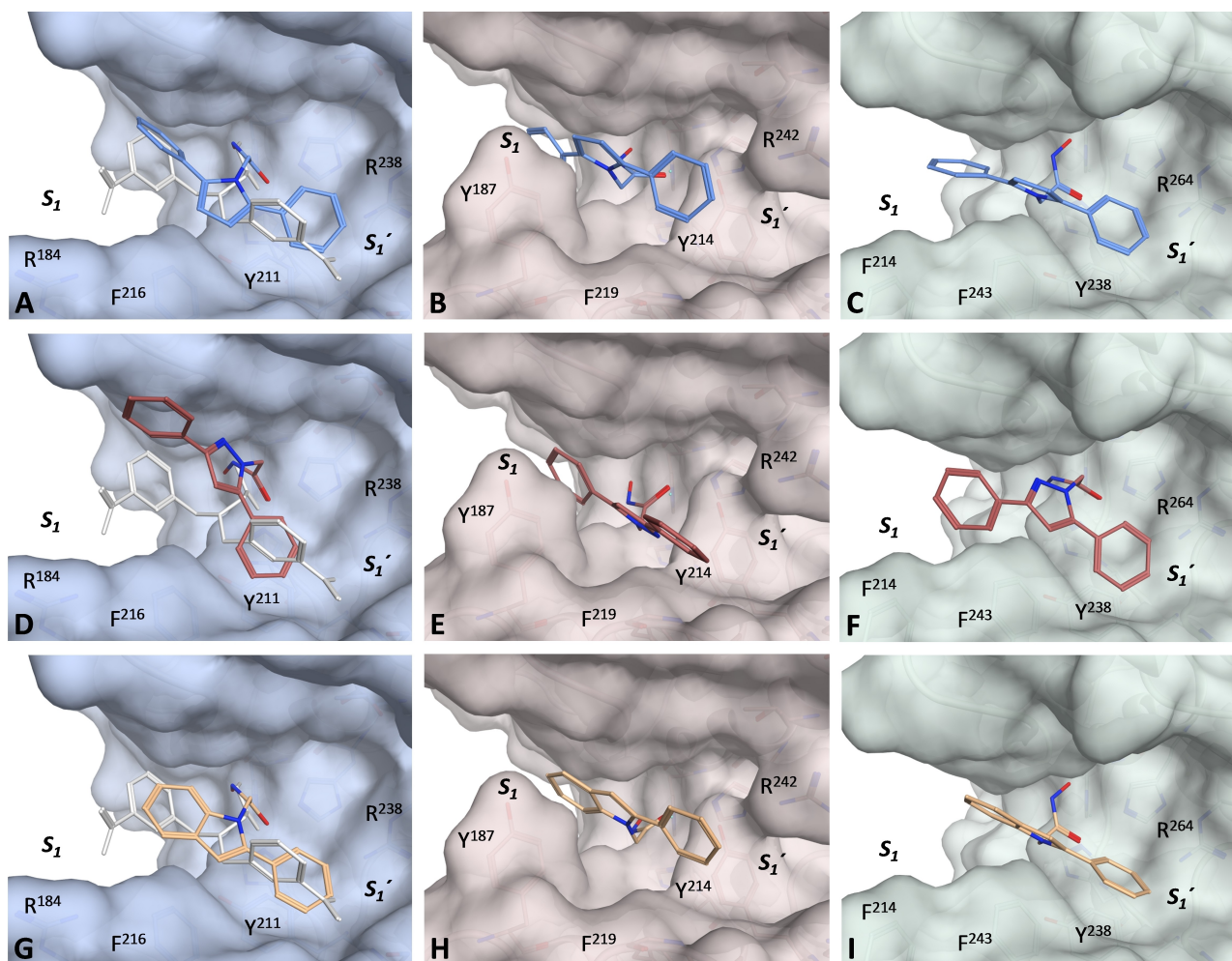


Figure 4. Docking of compounds with GOLD (Chemscore[®], 10 runs, top-ranked solutions) within the active site of meprin β : A) 2a, D) 3a, G) 4a, X-ray conformation of 1a in light grey, meprin α : B) 2a, E) 3a, H) 4a and ovastacin: C) 2a, F) 3a, I) 4a.

Taken together, the visual inspection of the docking experiments revealed in general a good fit of the putative inhibitors 2a, 3a and 4a within the active sites of meprin α , β and ovastacin, albeit compounds 2a and 4a seem to be able to address the S_1 and S_1' pockets slightly better than 3a, in particular based on the docking solutions found for meprin β . Hence, this would be in line with the results from the flexible alignments, that also suggested a better fit of 2a and 4a (vide supra). However, the docking experiments of the compounds with C_2 spacer (2b, 3b and 4b) yielded comparable poses (see the Supporting Information), although in this case the solutions of pyrazole 3b suggested a better fit within the active sites of meprin α and β , compared to the solutions of the respective derivative with shorter spacer (3a). Although none of the novel compounds completely matched the bioactive conformation of 1a, the *in silico* experiments indicated additional interactions, enabled by the introduction of the heteroaromatic core itself, that is, electrostatic interactions with Y^{211} or F^{216} in meprin β or the corresponding amino acids in meprin α and ovastacin, respectively. Hence, this might also contribute to improved ligand binding, rather than solely the fixation or rigidification of

the bioactive conformation of 1a. In particular the S_1 pockets of meprin α and ovastacin exhibit a lipophilic environment, since they are formed by Y^{187} and F^{214} , respectively. Thus, this creates a favorable environment for hydrophobic aryl moieties of the corresponding inhibitors, also corroborated by the docking solutions.

Summarized, the docking solutions and the results from the flexible alignments supported the idea of replacing the tertiary amine with heteroaromatic cores and we assumed that all of the proposed heteroaromatic inhibitors might be suitable replacements of the amine scaffold. Moreover, the *in silico* experiments indicated suitable binding modes for all the putative compounds, either with C_1 or C_2 spacer. Hence, we supposed that all of the aforementioned compounds could yield suitable scaffolds for the development of meprin α , meprin β and ovastacin inhibitors.

Due to the putative electrostatic interactions we also aimed at the exploration of the influence of the electrostatic properties of the heteroaromatic cores. Moreover, the introduction of nitrogen at different positions of the heteroaromatic cores, that is, "the necessary nitrogen", might have a huge impact on

pharmacodynamic and pharmacokinetic properties that might influence the further development of novel astacin proteinase inhibitors.^[15] Thus, we intended to introduce further five-membered heterocycles, i.e., isoxazole, pyrazole, 1,2,3-triazole, 1,2,4-triazole and imidazole, and further fused heteroaromatic cores, i.e. benzimidazole, imidazo[4,5-*b*]pyridines and indazole as novel scaffolds. This enabled the exploration of different electrostatic properties and also introduces different synthetic linchpins for further derivatization of the core structures as part of further optimization efforts.

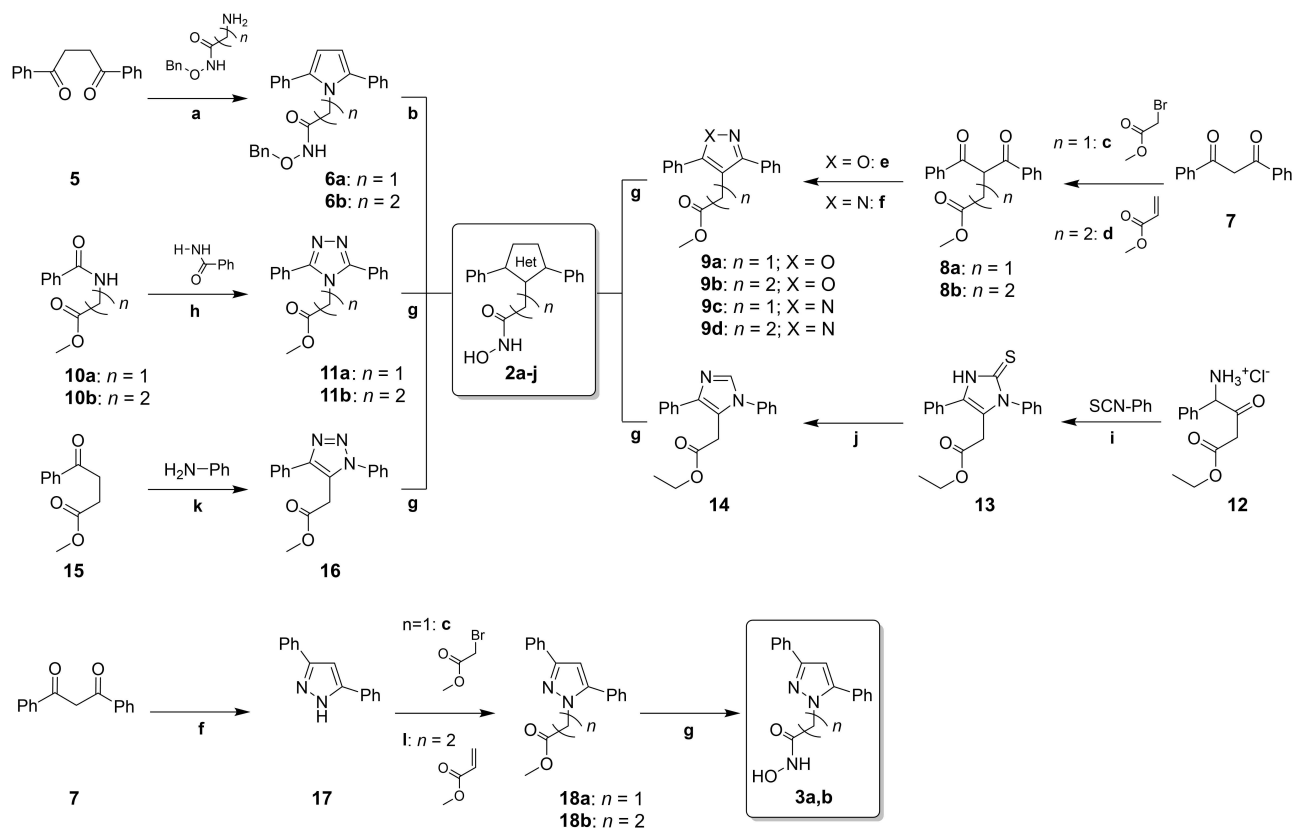
Chemistry

The synthesis of the monocyclic heteroaromatic compounds was accomplished as depicted in Scheme 1. The 2,5-diphenyl pyrrole derivatives **2a** and **b** were synthesized starting from 1,4-diphenylbutane-1,4-dione **5** by Paal–Knorr synthesis followed by deprotection of the benzylhydroxamic acid derivatives **6a** and **b**. The 3,5-diphenyl isoxazole- (**2c** and **d**) and the 3,5-diphenyl pyrazole-derivatives (**2e** and **f**) were synthesized from 1,3-diphenylpropane-1,3-dione **7**. After alkylation by either methyl bromoacetate or methyl acrylate, the isoxazoles **9a** and **b** were furnished by cyclocondensation of **8a** and **b** and hydroxylamine hydrochloride. Condensation of **8a** and **b** with hydrazine hydrate yielded the corresponding pyrazole deriva-

tives **9c** and **d**, respectively. Final aminolysis by means of hydroxyl amine hydrochloride furnished the hydroxamic acids **2c–f**.

The 3,5-diphenyl-1,2,4-triazoles (**2g** and **h**) were synthesized starting either from *N*-benzoyl glycine or *N*-benzoyl β -alanine, respectively.^[16] Reaction with 2-fluoropyridine, trifluoromethane-sulfonic acid anhydride and benzhydrazide under microwave conditions yielded the 1,2,4-triazole esters **11a** and **b** that were converted to this corresponding hydroxamic acids **2g** and **h** by means of hydroxyl amine hydrochloride. The imidazole **2i** was prepared starting from ethyl 4-amino-3-oxo-4-phenylbutanoate hydrochloride (**12**) that was acylated with phenylisothiocyanate followed by subsequent cyclization using pyridinium *para*-toluene sulfonate (PPTS), yielding thioimidazolidinone **13**.^[17] Desulfurization by means of hydrogen peroxide furnished imidazole ester **14**, that was finally converted to the corresponding hydroxamic acid **2i** by aminolysis using hydroxylamine hydrochloride. The 1,2,3-triazole derivative **2j** was synthesized from methyl 4-oxo-4-phenyl-butanoate (**15**) by copper mediated reaction with tosylhydrazide and aniline.^[18] The resulting methyl 1,4-diphenyl-1,2,3-triazol ester (**16**) was further treated with hydroxyl amine hydrochloride yielding compound **2j**.

The two 3,5-diphenyl pyrazoles **3a** & **b** were synthesized from 1,3-diphenylpropane-1,3-dione **7**, that was converted to pyrazole **17** by means of hydrazine hydrate. Alkylation with



Scheme 1. Synthesis of monocyclic heteroaromatic inhibitors. a) *p*TSA, THF/toluene (1:1, v/v), reflux, 23–50%; b) H₂, 4 bar, Pd/C, MeOH/THF (1:1, v/v), RT, 4–37%; c) NaH, DMF, 0 °C to RT, 73–100%; d) DBU, CH₂Cl₂, 0 °C to RT, 35%; e) NH₂OH·HCl, EtOH/water (3:2, v/v), μ W, 110 °C, 15–31%; f) N₂H₄·H₂O, EtOH/THF (2:1, v/v), RT, 58–99%; g) NH₂OH·HCl, NaOCH₃, MeOH, μ W, 80 °C, 19–66%; h) i: 2-fluoropyridine, Tf₂O, CH₂Cl₂, 0 °C, ii: μ W, 140 °C, 29–34%; i) TEA, EtOH, 50 °C, ii: PPTS, toluene, 120 °C, 48%; j) H₂O₂, AcOH, RT, 42%; k) i: tosylhydrazide, toluene, 80 °C, ii: Cu(OAc)₂, pivalic acid, 100 °C, 24%; l) DBU, MeCN, RT, 96%.

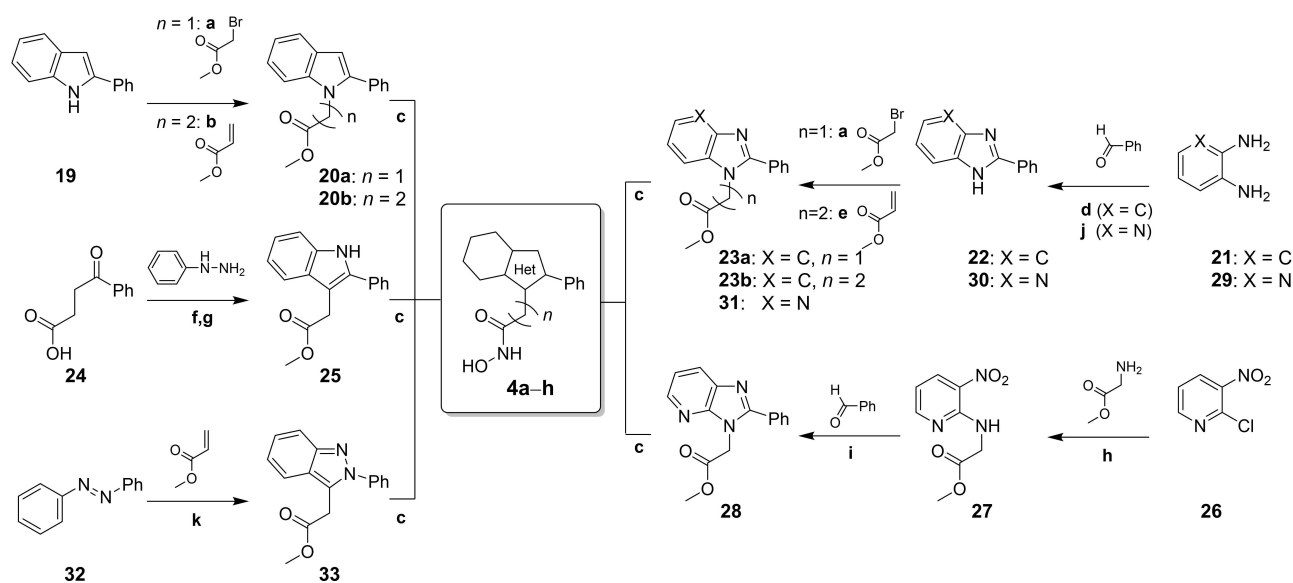
either methyl bromoacetate or methyl acrylate, respectively, yielded pyrazole esters **18a** and **b**, that were finally converted to corresponding hydroxamic acids **3a** and **b** by means of hydroxylamine hydrochloride.

The synthesis of the fused heteroaromatic inhibitors is depicted in scheme 2. The two *N*-alkyl indole derivatives **4a** and **b** were synthesized from 2-phenylindole (**19**), that was alkylated using either methyl bromoacetate or methyl acrylate, followed by aminolysis of the intermediate esters **20**. Benzimidazoles **4c** and **d** were synthesized starting from phenyl-1,2-diamine (**21**).^[19] Alkylation of the resulting 2-phenylbenzimidazole (**22**) with methyl bromoacetate or methyl acrylate led to benzimidazole esters **23a** and **b**, that were converted to the corresponding hydroxamic acids **4c** and **d** by means of hydroxylamine hydrochloride. The indole derivative **4e** was synthesized by Fischer indole synthesis from benzoylpropionic acid (**24**) and subsequent esterification, followed by aminolysis of the ester intermediate **25**. Imidazo[4,5-*b*]pyridine **4f** was synthesized by S_NAr reaction starting from 2-chloro-3-nitropyridine **26**.^[20] Reductive cyclization of **27** with benzaldehyde and sodium dithionite yielded ester intermediate **28**^[21], that was finally converted to hydroxamic acid **4f** by hydroxylaminolysis. The respective regioisomer **4g** was synthesized starting from 2,3-diaminopyridine **29**.^[22] Cyclization with benzaldehyde yielded imidazopyridine **30**. Alkylation with methyl bromoacetate, followed by separation of the isomers furnished ester intermediate **31** that was treated with hydroxylamine, yielding imidazo[4,5-*b*]pyridine **4g**. Finally, indazole **4h** was prepared from azobenzene **32**.^[23] Rhodium catalyzed reaction with methyl acrylate yielded **33** that was converted to the respective hydroxamate **4h** by hydroxylaminolysis.

Structure-activity relationships

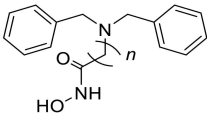
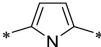
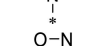
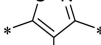
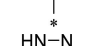
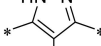
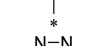
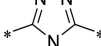
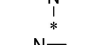
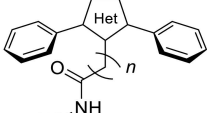
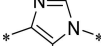
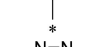

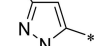
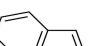
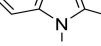
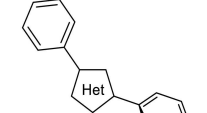
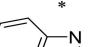
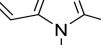
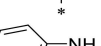
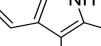
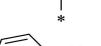
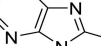
The synthesized inhibitors were first evaluated with regard to their ability to modulate meprin α and β activity (Table 1). The prototypic inhibitors of the "1,2,3-cyclization", that is, pyrroles **2a** and **2b**, exhibited a rather unexpected high activity compared to the reference inhibitors, based on the tertiary amine (**1d** and **1e**). The transition from the aliphatic tertiary amine to the heteroaromatic core led to an almost 400 fold increased K_i^{app} against meprin α of **2a** compared to **1d**. Although the activity of **2a** against meprin β is less pronounced, the scaffold-hopping yielded a compound with an activity in the micromolar range compared to an almost inactive tertiary amine counterpart (**1e**). The inhibitory activity of the corresponding compound bearing a C_2 spacer between hydroxamate and scaffold (**2b**) against meprin α and β is also increased compared to the respective tertiary amine derivative **1e**. However, the gain of activity for this compound is just twofold for meprin α and about fourfold for meprin β . Of note, the activity of **2a**, bearing a shorter spacer, is significantly higher compared to **2b**. This is contrary to the SAR found for the tertiary amine based inhibitors, where a longer spacer resulted in an increased activity against meprin α .^[13] This might also indicate a different binding mode, as already suggested by the *in silico* experiments (vide supra). The exploration of different heteroaromatic cores led to further improved potencies against meprin α and also meprin β , corroborating the potential π - π interactions of the heterocycles revealed by the docking studies.

The replacement of the central pyrrole of **2a** by an isoxazole (**2c**) led to a further 5-fold increase in activity against both proteinases, exhibiting a K_i^{app} in the lower one-digit nanomolar range against meprin α and a sub-micromolar K_i^{app} of 813 nM against meprin β , yielding an unprecedented 2000-fold im-



Scheme 2. Synthesis of fused heteroaromatic inhibitors. a) NaH, DMF, 0 °C to RT, 92–96%; b) DBU, MeCN, RT, 67%; c) $NH_2OH \cdot HCl$, $NaOCH_3$, μW , 80 °C, 15–66%; d) H_2O_2 , CAN, MeCN, μW , 50 °C, 53%; e) K_2CO_3 , MeCN, reflux, 66%; f) pTSA, $ZnCl_2$, AcOH, μW , 180 °C, 47%; g) MeOH, H_2SO_4 , reflux, 71%; h) TEA, DMF, μW , 120 °C, 94%; i) $Na_2S_2O_4$, DMF/EtOH (1:1, v/v), 80 °C, 36%; j) H_2O , reflux, 26%; k) $[Cp^*RhCl_2]_2$, $Cu(OAc)_2$, DMF, 130 °C, 13%.

Table 1. Inhibition of meprin α and β by five-membered and fused heteroaromatic hydroxamates.

scaffold	No	Het	n	K_i^{app} [nM]		SF ^[b]	
				Meprin α ^[a]	Meprin β ^[a]		
	1d ^[c]	–	1	7868 (1.04)	n.d. ^[d]	–	
	1e ^[c]	–	2	1647 (1.04)	74361 (1.04)	45	
	2a		1	20 (1.25)	4311 (1.09)	216	
	2b		2	736 (1.07)	15026 (1.08)	20	
	2c		1	4 (1.06)	813 (1.08)	203	
	2d		2	31 (1.09)	13491 (1.05)	435	
	2e		1	3 (1.04)	199 (1.05)	66	
	2f		2	76 (1.12)	8034 (1.07)	106	
	2g		1	66 (1.02)	8680 (1.04)	132	
	2h		2	306 (1.12)	42320 (1.09)	138	
	2i		1	2 (1.15)	443 (1.22)	222	
	2j		1	9 (1.01)	1448 (1.03)	161	
	3a		1	256 (1.08)	10440 (1.06)	41	
	3b		2	406 (1.09)	15411 (1.13)	38	
	4a		1	69 (1.08)	1076 (1.05)	16	
	4b		2	414 (1.02)	16990 (1.21)	41	
	4c		1	163 (1.14)	1625 (1.08)	10	
	4d		2	1031 (1.09)	27915 (1.05)	27	
	4e		1	82 (1.20)	1184 (1.02)	14	
	4f		1	262 (1.01)	4556 (1.12)	17	
	4g		1	1483 (1.35)	4170 (1.08)	3	
	4h		1	273 (1.13)	3364 (1.08)	12	
	Actinonin	–	–	–	8 (1.21)	219 (1.28)	27

[a] Geometric mean of three independent experiments with standard deviation factor. [b] SF: selectivity factor (K_i^{app} meprin β / K_i^{app} meprin α). [c] Data from ref. [12]. [d] Not determined, relative activity 82% @ 100 μ M

provement in potency against meprin α compared to the respective amine **1d**. Moreover, **2c** exhibits already a quite

favorable selectivity for meprin α over meprin β , i.e., by factor 200. The introduction of the C_2 spacer again led to a slightly

decreased activity of **2d** compared to **2c**. However, that decrease is even more pronounced with regard to meprin β inhibition. Thus, the selectivity for meprin α over β inhibition is even higher for **2d**, about factor 400. Although these compounds were originally designed just as novel scaffolds, the high activity of **2c** and **2d** against meprin α without further scaffold decoration in combination with the favorable selectivity over meprin β renders them as suitable probes for target validation, rather than just a scaffold for further derivatization. The same SAR-trend was also observed for the respective pyrazole derivatives **2e** and **f**, albeit the activity against meprin β was slightly higher than for the isoxazoles. However, the inhibitory activity of the respective 1,2,4-triazoles **2g** and **h** was slightly decreased compared to the isoxazoles, by factor 10, but still in the same range as the corresponding pyrroles **2a** and **b**. This might underpin the influence of the electrostatic properties of the heteroaromatic core on the inhibitory activity by affecting the putative π - π interactions found by the docking experiments (vide supra). Nevertheless, also **2g** and **h** are also far more potent compared to the tertiary amines **1d** and **e**. The activity of the imidazole **2i** and 1,2,3-triazole **2j** is again in the same activity range as the isoxazole **2c** or pyrazole **2e**, exemplifying for **2i** that also a basic heterocycle is tolerated, resembling also the basic properties of the tertiary amines.

The prototypic compounds for the "1,2,4-cyclization", that is, the pyrazoles **3a** and **b**, exhibited also increased activity compared to the corresponding tertiary amines **1d** and **e**, albeit to a smaller extent as the respective 1,2,3-cyclization compounds **2a**-**i**. This is in line with the results of the *in silico* experiments (vide supra), which also led to the conclusion that pyrazoles **3a** and **b** are less likely to meet the active conformation of tertiary amine **1a** and are less likely to address the S_1 and S_1' subpocket within the active site. A different binding mode is further corroborated by the missing influence of the spacer, since the corresponding inhibitors with either C_1 or C_2 spacer exhibit virtually the same activities. Finally, the compounds that were rigidified by means of ring fusion, i.e., indoles **4a** and **4b**, also exhibited increased activities compared to the tertiary amines **1d** and **e**. The gain of activity is in a comparable range as found for the pyrroles **2a** and **b**, respectively. The introduction of the C_2 spacer (**4b**) led to a reduced activity compared to the compound with C_1 spacer (**4a**), which is again contrary to the SAR of the tertiary amines but in line with the SAR of the 1,2,3-cyclized inhibitors **2a**-**h**. The introduction of an additional nitrogen (**4c**, **d** and **h**) or an altered indole substitution pattern (**4e**) had only marginal influence on the activity. However, the introduction of imidazopyridines (**4f** and **g**) affects in particular the activity dependent on the substitution pattern, underpinning a potential influence of the electrostatic properties of the heterocyclic cores.

Following the inhibitor evaluation with meprin α and β , selected compounds were investigated regarding their inhibitory activity against ovastacin (Table 2). Except triazole **2h**, all of the tested compounds exhibited also activities in the lower micromolar (**2f**, **g**; **3a**, **b**; **4b**, **c**, **d**) or even nanomolar range (**2c**, **e** and **4a**). Although the inhibitory activities are lower

Table 2. Inhibition of ovastacin by selected inhibitors.

Cmpd.	K_i^{app} [nM]	SF	
		Meprin α ^[a]	Meprin β ^[b]
2c	66 (1.09)	17	0.1
2e	196 (1.19)	65	1
2f	2423 (1.04)	32	0.3
2g	4877 (1.06)	74	0.6
2h	31799 (1.01)	104	0.8
3a	1045 (1.01)	4	0.1
3b	1096 (1.07)	3	0.1
4a	93 (1.19)	1.3	0.1
4b	1300 (1.09)	3.1	0.1
4c	2090 (1.02)	13	1.3
4d	9798 (1.06)	9.5	0.4

[a] Selectivity factor (K_i^{app} ovastacin/ K_i^{app} meprin α); [b] Selectivity factor (K_i^{app} ovastacin/ K_i^{app} meprin β)

compared to meprin α , they are in the same range or even better than found for meprin β , rendering these compounds also as highly suitable scaffolds for the further development of ovastacin inhibitors. In particular, the compounds obtained by "1,2,3-cyclization" exhibit favorable inhibition properties. Of note, isoxazole **2c**, pyrazole **2e** and indole **4a** exhibit even higher activities without any scaffold decoration as the recently reported tertiary amine based ovastacin inhibitors.^[14] Thus, these compounds are the most potent small molecule ovastacin inhibitors reported to date.

Finally, the inhibition of exemplary proteases belonging to the metzincin target family, that is, ADAMs and MMPs, was evaluated (Table 3). The selected inhibitors exhibited a slightly less favorable selectivity profile compared to the tertiary amines reported recently,^[12] showing some inhibition of individual proteases at a concentration of 200 μM . Nevertheless, all tested compounds exhibited only little inhibition of the off-target proteinases at a lower concentration of 10 μM . Thus, these heteroaromatic cores could be considered as suitable scaffolds for the development of astacin inhibitors, without significant off-target inhibition liabilities, per se. With regard to the high potency of compounds **2c** and **e** against meprin α in the low nanomolar range, the low off-target inhibition at 10 μM results in a selectivity factor >10000 , supporting their suitability as chemical probes for meprin α target validation. Moreover, none of the tested compounds suffered from cytotoxicity issues, exemplified by the cell viability of liver and neuronal cell lines (Table 3).

Conclusion

Proteinases of the astacin family are increasingly getting into the focus of drug discovery. In particular, the inhibition of meprin α and β , as well as ovastacin offers novel treatment options for kidney diseases, fibrosis, cancer or infertility, respectively. Recently, the first potent and selective inhibitors of meprins and ovastacin have been reported, based on a tertiary amine scaffold. Albeit this scaffold exhibits favorable *in vitro* properties, it also exhibits several potential liabilities, such as

Table 3. Inhibition of off-target proteinases and *in vitro* toxicity of selected compounds.

	C_{compound} [μM]	2a	2c	Relative enzyme activity [%]					
				2d	2e	2f	2g	4a	4c
MMP2	10	83	87	98	104	97	95	85	89
	200	1	34	74	61	77	70	41	46
MMP9	10	92	86	89	81	93	99	90	96
	200	1	16	39	27	65	54	53	68
MMP13	10	79	80	79	75	93	93	77	102
	200	5	31	66	67	68	76	54	72
ADAM10	10	82	80	75	73	66	89	89	87
	200	29	22	21	23	12	83	68	76
ADAM17	10	82	62	75	61	76	90	88	92
	200	25	9	24	7	27	56	56	56
Cell viability [%]									
HepG2	30	n.t.	85	90	100	93	94	n.t.	85
SY-5Y	30	n.t.	96	123	92	93	99	n.t.	94

n.t.: not tested

metabolic instability or also entropic unfavorable binding to the target due to the high conformational flexibility. The latter issue was addressed by a rigidification and scaffold-hopping approach within this study, yielding novel astacin inhibitors with heteroaromatic scaffolds.

Thus, the formal cyclization of the tertiary amine resulted in an unprecedented increase in activity against meprin α and β . Moreover, selected compounds also exhibited favorable inhibition of ovastacin. The novel heteroaromatic scaffolds did not show marked inhibition of related metalloproteinases, nor cytotoxic effects, rendering them very suitable starting points for further medicinal chemistry exploration and optimization. However, already at this stage – without any functionalization or decoration – some compounds exhibited remarkable high potency against meprin α accompanied with a favorable selectivity over meprin β . Hence, these inhibitors could be directly used as chemical probes for target validation purposes of meprin α , for example, in the context of cancer, as a more suitable replacement for the commonly utilized less selective broadspectrum metallo-proteinase inhibitor actinonin.

Experimental Section

Chemistry

General. Starting materials and solvents were purchased from Aldrich, Activate Scientific, Alfa Aesar and Merck Millipore. The purity of the compounds was assessed by HPLC and confirmed to be $\geq 95\%$. The analytical HPLC-system consisted of a Merck–Hitachi device (model LaChrom) utilizing a Phenomenex Luna 5 μM C18(2) column (125 mm \times 4.0 mm) with $\lambda = 214$ nm as the reporting wavelength. The compounds were analyzed using a gradient at a flow rate of 1 mL/min, whereby eluent (A) was acetonitrile, eluent (B) was water, both containing 0.04% (v/v) trifluoro acetic acid applying the following gradient: 0–5 min: 5% (A), 5–15 min: 5 \rightarrow 60% (A), 15–20 min: 60 \rightarrow 95% (A), 20–30 min: 95% (A); gradient 2: 0–15 min: 5 \rightarrow 50% (A), 15–20 min: 50 \rightarrow 95% (A), 20–23 min: 95% (A). The purities of all reported compounds were determined by the percentage of the peak area at 214 nm. ESI or APCI mass spectra were obtained with an Expression CMS spectrometer (Advion). The

high-resolution positive ion ESI mass spectra were obtained from a LTQ Orbitrap XL (Thermo Fisher Scientific). The NMR spectra were recorded at a DDR2 400 spectrometer (Agilent) and an Avancell-System (Bruker Biospin GmbH). $[\text{D}_6]\text{DMSO}$ was used as solvent unless otherwise specified. Chemical shifts are expressed as parts per million (ppm). The solvent was used as internal standard. Splitting patterns have been designated as follows: s (singlet), d (doublet), dd (doublet of doublet), t (triplet), m (multiplet), and br (broad signal). Semi preparative HPLC was performed on a Prepstar device (Varian) equipped with a Phenomenex Luna 10 μM C18(2) column (250 mm \times 21 mm). The compounds were eluted using the same solvent system as described above, applying a flow rate of 21 mL/min.

General method for deprotection of hydroxamic acids by hydrogenation: The respective benzyl-protected hydroxamic acid derivative was dissolved in MeOH/THF (1:1, v/v, 10 mL). Palladium on charcoal was added and the vial was purged with hydrogen. After 4 h at 4 bar, the mixture was filtered through celite and evaporated. The residue was purified by semi-preparative HPLC.

2-(2,5-Diphenylpyrrol-1-yl)ethanehydroxamic acid (2a): The compound was synthesized from *O*-benzyl-2-(2,5-diphenylpyrrol-1-yl) ethane-hydroxamic acid (6a, 90 mg, 0.24 mmol, 1 equiv) as described above. Yield: 25 mg (37%); ESI-MS: m/z 293.2 $[M+H]^+$; HPLC: $t_R = 15.84$ min (97.7%); ^1H NMR (400 MHz, $[\text{D}_6]\text{DMSO}$): $\delta = 4.34$ (s, 1.5H), 4.65 (s, 0.5H), 6.27 (s, 2H), 7.33–7.36 (m, 2H), 7.41–7.47 (m, 8H), 8.99 (br s, 0.6H), 9.19 (br s, 0.2H), 10.26 (br s, 0.2H), 10.54 (br s, 0.8H) mixture of *cis-trans* isomers; ^{13}C NMR (176 MHz, $[\text{D}_6]\text{DMSO}$): $\delta = 46.2, 109.6, 127.6, 128.7, 128.9, 129.0, 133.5, 137.1, 166.4$; HRMS m/z : 315.1114 $[M+Na]^+$, calcd for $\text{C}_{18}\text{H}_{16}\text{N}_2\text{NaO}_2^+$: 315.1104.

3-(2,5-Diphenylpyrrol-1-yl)propanehydroxamic acid (2b): The compound was synthesized from *O*-benzyl-3-(2,5-diphenylpyrrol-1-yl)-propanehydroxamic acid (6b, 300 mg, 0.76 mmol, 1 equiv) as described above. Yield: 9 mg (4%); ESI-MS: m/z 307.4 $[M+H]^+$, 329.4 $[M+Na]^+$; HPLC: $t_R = 16.27$ min ($>99\%$); ^1H NMR (400 MHz, $[\text{D}_6]\text{DMSO}$): $\delta = 1.83$ –1.87 (m, 1.8H), 2.09–2.13 (m, 0.2H), 4.28–4.32 (m, 2H), 6.23 (s, 2H), 7.34–7.38 (m, 2H), 7.44–7.51 (m, 8H), 8.57 (br s, 0.6H), 8.81 (br s, 0.1H), 9.76 (br s, 0.1H), 10.16 (br s, 0.9H) mixture of *cis-trans* isomers; HRMS m/z : 329.1273 $[M+Na]^+$, calcd for $\text{C}_{19}\text{H}_{18}\text{N}_2\text{NaO}_2^+$: 329.1260.

General method for the synthesis of hydroxamic acids from carboxylic acid esters: The respective ester derivative (1 equiv) was dissolved in MeOH (5 mL), treated with NaOCH_3 (6 equiv) and

hydroxylamine hydrochloride (3 equiv). The mixture was heated in a microwave at 80 °C for 10 minutes. The volatiles were evaporated. The remains were taken up in water, acidified by means of diluted aqueous HCl and extracted with EtOAc (3 × 25 mL). The combined organic layers were dried over Na₂SO₄ and evaporated. The residue was purified by semi-preparative HPLC.

2-(3,5-Diphenylisoxazol-4-yl)ethanehydroxamic acid (2c): The compound was synthesized from methyl 2-(3,5-diphenylisoxazol-4-yl)acetate (9a, 92 mg, 0.31 mmol, 1 equiv) as described above. Yield: 32 mg (35%); ESI-MS: *m/z* 295.1 [M+H]⁺, 317.2 [M+Na]⁺; HPLC: *t_R* = 14.56 min (> 99%); ¹H NMR (400 MHz, [D₆]DMSO): δ = 3.41 (s, 2H), 7.55–7.62 (m, 6H), 7.68–7.70 (m, 2H), 7.79–7.82 (m, 2H), 10.77 (s, 1H); ¹³C NMR (176 MHz, [D₆]DMSO): δ = 27.4, 108.2, 127.5, 127.8, 128.5, 128.7, 129.1, 129.4, 129.7, 130.3, 130.8, 164.2, 166.6, 167.6; HRMS *m/z*: 317.0907 [M+Na]⁺, calcd for C₁₇H₁₄N₂NaO₃⁺: 317.0897.

3-(3,5-Diphenylisoxazol-4-yl)propanehydroxamic acid (2d): The compound was synthesized from methyl 3-(3,5-diphenylisoxazol-4-yl)propanoate (9b, 49 mg, 0.16 mmol) as described above. Yield: 11 mg (22%); ESI-MS: *m/z* 309.4 [M+H]⁺, 331.4 [M+Na]⁺; HPLC: *t_R* = 14.93 min (> 99%); ¹H NMR (400 MHz, [D₆]DMSO): δ = 2.09–2.13 (m, 2H), 2.95–2.99 (m, 2H), 7.57–7.63 (m, 2H), 7.69–7.71 (m, 2H), 7.81–7.84 (m, 2H), 10.36 (br s, 1H); ¹³C NMR (176 MHz, [D₆]DMSO): δ = 28.42, 108.45, 127.79, 128.03, 128.29, 129.08, 168.31; HRMS *m/z*: 294.1251 [M+H]⁺, calcd for C₁₇H₁₆N₃O₂⁺: 294.1237.

2-(3,5-Diphenyl-1H-pyrazol-4-yl)ethanehydroxamic acid (2e): The compound was synthesized from methyl 2-(3,5-diphenyl-1H-pyrazol-4-yl)acetate (9c, 209 mg, 0.72 mmol, 1 equiv) as described above. Yield: 83 mg (40%); ESI-MS: *m/z* 294.5 [M+H]⁺; HPLC: *t_R* = 12.03 min (> 99%); ¹H NMR (400 MHz, [D₆]DMSO): δ = 3.32 (s, 1.8H), 3.63 (s, 0.2H), 7.38–7.42 (m, 2H), 7.46–7.49 (m, 4H), 7.64–7.66 (m, 4H), 10.09 (br s, 0.1H), 10.62 (br s, 0.9H) mixture of *cis-trans* isomers; ¹³C NMR (176 MHz, [D₆]DMSO): δ = 28.4, 108.5, 127.8, 128.0, 128.3, 129.1, 168.3; HRMS *m/z*: 294.1251 [M+H]⁺, calcd for C₁₇H₁₆N₃O₂⁺: 294.1237.

3-(3,5-Diphenyl-1H-pyrazol-4-yl)propanehydroxamic acid (2f): The compound was synthesized from methyl 3-(3,5-diphenyl-1H-pyrazol-4-yl)propanoate (9d, 306 mg, 1 mmol, 1 equiv) as described above. Yield: 58 mg (19%); ESI-MS: *m/z* 308.4 [M+H]⁺; HPLC: *t_R* = 15.52 min (96.8%); ¹H NMR (400 MHz, [D₆]DMSO): δ = 2.06–2.11 (m, 2H), 2.93–2.97 (m, 2H), 7.41 (t, 2H, ³J = 7.3 Hz), 7.50 (t, 4H, ³J = 7.6 Hz), 7.64 (d, 4H, ³J = 7.8 Hz), 10.33 (br s, 1H); ¹³C NMR (176 MHz, [D₆]DMSO): δ = 20.0, 33.5, 114.1, 128.0, 128.2, 129.2, 168.7; HRMS *m/z*: 308.1409 [M+H]⁺, calcd for C₁₈H₁₈N₃O₂⁺: 308.1394.

2-(3,5-Diphenyl-1,2,4-triazol-4-yl)ethanehydroxamic acid (2g): The compound was synthesized from methyl 2-(3,5-diphenyl-4H-1,2,4-triazol-4-yl)acetate (11a, 86 mg, 0.29 mmol, 1 equiv) as described above. Yield: 45 mg (53%); ESI-MS: *m/z* 295.3 [M+H]⁺; HPLC: *t_R* = 7.73 min (98.2%); ¹H NMR (400 MHz, [D₆]DMSO): δ = 4.56 (s, 1.5 H), 4.85 (s, 0.5 H), 7.58–7.70 (m, 10 H), 10.50 (br s, 0.3 H), 10.81 (br s, 0.7 H) mixture of *cis-trans* isomers; ¹³C NMR (176 MHz, [D₆]DMSO): δ = 45.5, 127.6, 129.0, 129.2, 129.4, 129.5, 130.6, 155.9, 164.0; HRMS *m/z*: 295.1204 [M+H]⁺, calcd for C₁₆H₁₅N₄O₂⁺: 295.1190.

3-(3,5-Diphenyl-1,2,4-triazol-4-yl)propanehydroxamic acid (2h): The compound was synthesized from methyl 3-(3,5-diphenyl-4H-1,2,4-triazol-4-yl)propanoate (11b, 39 mg, 0.34 mmol, 1 equiv) as described above. Yield: 39 mg (37%); ESI-MS: *m/z* 309.4 [M+H]⁺; HPLC: *t_R* = 8.59 min (97.0%); ¹H NMR (400 MHz, [D₆]DMSO): δ = 2.10 (t, 2H, ³J = 7.6 Hz), 4.39 (t, 2H, ³J = 7.5 Hz), 7.61–7.63 (m, 6H), 7.75–7.78 (m, 4H), 9.89 (br s, 0.1H), 10.28 (br s, 0.9H) mixture of *cis-trans* isomers; ¹³C NMR (176 MHz, [D₆]DMSO): δ = 31.4, 41.5, 127.5, 129.4, 129.5, 130.8, 155.0, 165.9; HRMS *m/z*: 309.1358 [M+H]⁺, calcd for C₁₇H₁₇N₄O₂⁺: 309.1346.

2-(3,5-Diphenylimidazol-4-yl)ethanehydroxamic acid (2i): The compound was synthesized from ethyl 2-(3,5-diphenylimidazol-4-yl)acetate (14, 89 mg, 0.29 mmol, 1 equiv) as described above. Yield: 34 mg (39%); ESI-MS: *m/z* 294.1 [M+H]⁺; HPLC: *t_R* = 6.51 min (> 99%); ¹H NMR (400 MHz, [D₆]DMSO): δ = 3.47 (s, 1.7H), 3.77 (s, 0.3H), 7.44–7.47 (m, 1H), 7.51–7.69 (m, 9H), 8.88 (br s, 0.1H), 9.32 (br s, 0.1H), 10.25 (s, 0.2H), 10.61 (s, 0.8H) mixture of *cis-trans* isomers; ¹³C NMR (176 MHz, [D₆]DMSO): δ = 28.1, 124.4, 126.9, 128.2, 129.2, 129.5, 129.6, 130.3, 130.5, 134.6, 137.1, 158.6, 165.2; HRMS *m/z*: 294.1231 [M+H]⁺, calcd for C₁₇H₁₆N₃O₂⁺: 294.1237.

2-(3,5-Diphenyl-1,2,3-triazol-4-yl)ethanehydroxamic acid (2j): The compound was synthesized from methyl 2-(3,5-diphenyl-1,2,3-triazol-4-yl)acetate (16, 70 mg, 0.24 mmol, 1 equiv) as described above. Yield: 23 mg (32%); ESI-MS: *m/z* 295.1 [M+H]⁺; HPLC: *t_R* = 10.43 min (> 99%); ¹H NMR (400 MHz, [D₆]DMSO): δ = 3.63 (s, 1.7H), 3.92 (s, 0.3H), 7.42–7.45 (m, 1H), 7.52 (t, 2H, ³J = 7.8 Hz), 7.57–7.69 (m, 5H), 7.75–7.77 (m, 2H), 9.04 (br s, 0.6H), 9.39 (br s, 0.2H), 10.33 (s, 0.1H), 10.76 (s, 0.9H) mixture of *cis-trans* isomers; ¹³C NMR (176 MHz, [D₆]DMSO): δ = 28.1, 125.9, 126.1, 127.2, 127.4, 128.6, 129.2, 129.3, 130.2, 130.4, 131.3, 136.3, 145.5, 164.9; HRMS *m/z*: 295.1207 [M+H]⁺, calcd for C₁₆H₁₅N₄O₂⁺: 295.1190.

2-(3,5-Diphenylpyrazol-1-yl)ethanehydroxamic acid (3a): The compound was synthesized from methyl 2-(3,5-diphenyl-1H-pyrazol-1-yl)acetate (18a, 247 mg, 0.84 mmol, 1 equiv) as described above. Yield: 141 mg (57%); ESI-MS: *m/z* 294.4 [M+H]⁺; HPLC: *t_R* = 15.63 min (97.5%); ¹H NMR (400 MHz, [D₆]DMSO): δ = 4.68 (s, 1.8H), 5.04 (br s, 0.2H), 6.91 (s, 1H), 7.31–7.35 (m, 1H), 7.41–7.55 (m, 5H), 7.65–7.68 (m, 2H), 7.83–7.85 (m, 2H), 9.12 (br s, 0.9H), 9.36 (br s, 0.1H), 10.35 (br s, 0.1H), 10.93 (br s, 0.9H) mixture of *cis-trans* isomers; ¹³C NMR (176 MHz, [D₆]DMSO): δ = 50.4, 103.7, 125.6, 128.2, 129.1, 129.2, 129.3, 130.4, 133.5, 146.4, 150.3, 164.4; HRMS *m/z*: 294.1251 [M+H]⁺, calcd for C₁₇H₁₆N₃O₂⁺: 294.1237.

3-(3,5-Diphenylpyrazol-1-yl)propanehydroxamic acid (3b): The compound was synthesized from methyl 3-(3,5-diphenyl-1H-pyrazol-1-yl)propanoate (18b, 259 mg, 0.84 mmol, 1 equiv) as described above. Yield: 171 mg (66%); ESI-MS: *m/z* 308.4 [M+H]⁺; HPLC: *t_R* = 17.68 min (> 99%); ¹H NMR (400 MHz, [D₆]DMSO): δ = 2.66 (t, 2H, ³J = 7.2 Hz), 4.32 (t, 2H, ³J = 7.2 Hz), 6.84 (s, 1H), 7.30–7.34 (m, 1H), 7.41–7.45 (m, 2H), 7.47–7.57 (m, 3H), 7.60–7.63 (m, 2H), 7.84–7.86 (m, 2H), 9.97 (br s, 0.1H), 10.53 (br s, 0.9H) mixture of *cis-trans* isomers; ¹³C NMR (176 MHz, [D₆]DMSO): δ = 33.0, 45.6, 130.8, 125.6, 128.0, 129.1, 129.1, 129.2, 129.3, 130.5, 133.7, 145.2, 149.9, 166.8; HRMS *m/z*: 330.1223 [M+Na]⁺, calcd for C₁₈H₁₇N₃NaO₂⁺: 330.1213.

2-(2-Phenylindol-1-yl)ethanehydroxamic acid (4a): The compound was synthesized from methyl 2-(2-phenyl-1H-indol-1-yl)acetate (20a, 265 mg, 1 mmol, 1 equiv) as described above. Yield: 91 mg (34%); ESI-MS: *m/z* 267.3 [M+H]⁺; HPLC: *t_R* = 15.81 min (> 99%); ¹H NMR (400 MHz, [D₆]DMSO): δ = 4.66 (s, 1.7H), 4.99 (s, 0.3H), 6.58 (s, 1H), 7.08–7.12 (m, 1H), 7.16–7.20 (m, 1H), 7.36–7.38 (m, 1H), 7.43–7.47 (m, 1H), 7.49–7.53 (m, 2H), 7.58–7.64 (m, 3H), 10.34 (s, 0.1H), 10.93 (s, 0.9H) mixture of *cis-trans* isomers; ¹³C NMR (176 MHz, [D₆]DMSO): δ = 44.9, 102.2, 110.7, 120.4, 120.6, 122.0, 128.1, 128.6, 129.2, 129.6, 132.5, 138.5, 142.0, 165.3; HRMS *m/z*: 289.0960 [M+Na]⁺, calcd for C₁₆H₁₄N₂NaO₂⁺: 289.0947.

3-(2-Phenylindol-1-yl)propanehydroxamic acid (4b): The compound was synthesized from methyl 2-(2-phenyl-1H-indol-1-yl)acetate (20b, 188 mg, 0.67 mmol, 1 equiv) as described above. Yield: 33 mg (18%); ESI-MS: *m/z* 281.2 [M+H]⁺; HPLC: *t_R* = 15.22 min (> 99%); ¹H NMR (400 MHz, [D₆]DMSO): δ = 2.34–2.38 (m, 2H), 4.36–4.40 (m, 2H), 6.54 (s, 1H), 7.07–7.10 (m, 1H), 7.18–7.22 (m, 1H), 7.45–7.49 (m, 1H), 7.51–7.58 (m, 6H), 9.97 (br s, 0.1H), 10.46 (br s, 0.9H) mixture of *cis-trans* isomers; ¹³C NMR (176 MHz, [D₆]DMSO): δ = 33.3, 40.6, 102.6, 111.0, 120.7, 122.1, 128.2, 128.6, 129.2, 129.6,

132.7, 137.5, 141.1, 166.7; HRMS m/z : 281.1301 $[M+H]^+$, calcd for $C_{17}H_{17}N_2O_2^+$: 281.1285.

2-(2-Phenylbenzimidazol-1-yl)ethanehydroxamic acid (4c): The compound was synthesized from methyl 2-(2-phenyl-1*H*-benzimidazol-1-yl)acetate (23a, 134 mg, 0.5 mmol, 1 equiv) as described above. Yield: 88 mg (66%); ESI-MS: m/z 268.3 $[M+H]^+$; HPLC: t_R = 5.96 min (>99%); 1H NMR (400 MHz, $[D_6]DMSO$): δ = 4.95 (s, 1.6 H), 5.29 (s, 0.4 H), 7.44–7.51 (m, 2H), 7.64–7.71 (m, 4H), 7.78–7.84 (m, 1H), 7.88–7.90 (m, 2H), 10.62 (br s, 0.2H), 11.10 (br s, 0.8 H) mixture of *cis-trans* isomers; ^{13}C NMR (176 MHz, $[D_6]DMSO$): δ = 45.9, 112.4, 117.4, 125.1, 129.6, 129.8, 129.9, 130.2, 132.1, 134.9, 136.0, 152.8, 158.9, 163.3; HRMS m/z : 268.1092 $[M+H]^+$, calcd for $C_{15}H_{14}N_3O_2^+$: 268.1081.

3-(2-Phenylbenzimidazol-1-yl)propanehydroxamic acid (4d): The compound was synthesized from methyl 2-(2-phenyl-1*H*-benzimidazol-1-yl)propanoate (23b, 88 mg, 0.31 mmol, 1 equiv) as described above. Yield: 33 mg (37%); ESI-MS: m/z 282.4 $[M+H]^+$; HPLC: t_R = 6.61 min (95.7%); 1H NMR (400 MHz, $[D_6]DMSO$): δ = 2.59 (t, 2H, 3J = 7.4 Hz), 4.60 (t, 2H, 3J = 7.7 Hz), 7.49–7.57 (m, 2H), 7.67–7.74 (m, 3H), 7.80–7.83 (m, 1H), 7.87–7.89 (m, 2H), 7.93–7.95 (m, 1H), 10.05 (br s, 0.1H), 10.50 (br s, 0.9H) mixture of *cis-trans* isomers; ^{13}C NMR (176 MHz, $[D_6]DMSO$): δ = 32.1, 42.4, 113.2, 116.7, 125.6, 129.6, 130.7, 132.2, 134.3, 151.9, 158.5, 158.9, 166.1; HRMS m/z : 282.1248 $[M+H]^+$, calcd for $C_{16}H_{16}N_3O_2^+$: 282.1237.

2-(2-Phenyl-1*H*-indol-3-yl)ethanehydroxamic acid (4e): The compound was synthesized from methyl 2-(2-phenyl-1*H*-indol-3-yl)acetate (25, 89 mg, 0.34 mmol, 1 equiv) as described above. Yield: 14 mg (15%); ESI-MS: m/z 267.2 $[M+H]^+$, 206.1 $[M-CH_2NO_2]^+$; HPLC: t_R = 11.97 min (>99%); 1H NMR (400 MHz, $[D_6]DMSO$): δ = 3.51 (s, 1.9H), 3.85 (s, 0.1H), 7.02 (t, 1H, 3J = 7.6 Hz), 7.12 (t, 1H, 3J = 7.5 Hz), 7.36–7.42 (m, 2H), 7.51 (t, 2H, 3J = 7.7 Hz), 7.61 (d, 1H, 3J = 7.8 Hz), 7.87 (d, 2H, 3J = 7.8 Hz), 10.77 (s, 1H), 11.26 (s, 1H) mixture of *cis-trans* isomers; ^{13}C NMR (176 MHz, CD_3OD): δ = 29.0, 103.8, 110.7, 118.1, 119.4, 121.6, 127.4, 128.0, 128.4, 128.9, 132.8, 136.4, 136.7, 170.3; HRMS m/z : 289.0959 $[M+Na]^+$, calcd for $C_{16}H_{14}N_2NaO_2^+$: 289.0947.

2-(2-Phenylimidazo[4,5-*b*]pyridin-3-yl)ethanehydroxamic acid (4f): The compound was synthesized from methyl 2-(2-phenyl-3*H*-imidazo[4,5-*b*]pyridin-3-yl)acetate (28, 90 mg, 0.34 mmol, 1 equiv) as described above. Yield: 35 mg (39%); ESI-MS: m/z 269.1 $[M+H]^+$; HPLC: t_R = 6.75 min (>99%); 1H NMR (400 MHz, $[D_6]DMSO$): δ = 4.92 (s, 1.6H), 5.26 (s, 0.4H), 7.36–7.39 (m, 1H), 7.58–7.61 (m, 3H), 7.78–7.80 (m, 0.5H), 7.87–7.89 (m, 1.5H), 8.14–8.16 (dd, 1H, 3J = 7.8 Hz, 4J = 1.2 Hz), 8.38–8.89 (m, 1H), 9.53 (br s, 0.2H), 10.45 (s, 0.2H), 11.01 (s, 0.8H) mixture of *cis-trans* isomers; ^{13}C NMR (176 MHz, $[D_6]DMSO$): δ = 43.3, 119.5, 127.2, 129.3, 129.6, 129.8, 130.9, 134.7, 144.6, 148.8, 154.9, 164.2; HRMS m/z : 269.1046 $[M+H]^+$, calcd for $C_{14}H_{13}N_4O_2^+$: 269.1033.

2-(2-Phenylimidazo[4,5-*b*]pyridin-1-yl)ethanehydroxamic acid (4g): The compound was synthesized from methyl 2-(2-phenyl-1*H*-imidazo[4,5-*b*]pyridin-1-yl)acetate (31, 185 mg, 0.69 mmol, 1 equiv) as described above. Yield: 38 mg (20%); ESI-MS: m/z 269.1 $[M+H]^+$; HPLC: t_R = 6.61 min (>99%); 1H NMR (400 MHz, $[D_6]DMSO$): δ = 5.54 (s, 1.4H), 5.86 (s, 0.6H), 7.69–7.71 (m, 3H), 7.98 (t, 1H, 3J = 7.1 Hz), 8.32–8.34 (m, 2H), 8.73–8.79 (m, 2H), 9.32 (br s, 0.7H), 9.84 (br s, 0.3H), 10.80 (s, 0.3H), 11.27 (s, 0.7H) mixture of *cis-trans* isomers; ^{13}C NMR (176 MHz, $[D_6]DMSO$): δ = 53.7, 118.6, 120.1, 128.6, 129.4, 130.0, 133.3, 139.7, 149.4, 158.6, 158.8, 159.1, 162.0; HRMS m/z : 269.1028 $[M+H]^+$, calcd for $C_{14}H_{13}N_4O_2^+$: 269.1033.

2-(2-Phenylindazol-3-yl)ethanehydroxamic acid (4h): The compound was synthesized from methyl 2-(2-phenyl-2*H*-indazol-3-yl)acetate (33, 32 mg, 0.12 mmol, 1 equiv) as described above. Yield: 18 mg (56%); ESI-MS: m/z 268.1 $[M+H]^+$; HPLC: t_R = 9.49 min (>

99%); 1H NMR (400 MHz, $[D_6]DMSO$): δ = 3.83 (s, 1.8H), 4.15 (s, 0.2H), 7.08–7.11 (m, 1H), 7.30–7.34 (m, 1H), 7.55–7.66 (m, 4H), 7.72–7.78 (m, 3H), 10.21 (s, 0.1H), 10.86 (s, 0.9H) mixture of *cis-trans* isomers; ^{13}C NMR (176 MHz, CD_3OD): δ = 29.0, 116.3, 119.9, 121.6, 126.3, 127.2, 129.1, 129.4, 130.2, 139.0, 148.3, 166.3; HRMS m/z : 268.1097 $[M+H]^+$, calcd for $C_{15}H_{14}N_3O_2^+$, 268.1081.

Flexible alignment: The flexible alignments were performed with Molecular Operating Environment (MOE), v2018.01; (Chemical Computing Group). Compound 1a was extracted from the PDB file of the co-crystal structure with meprin β (internal communication; PDB ID: 7AQ1) The carboxylic acids were deleted manually and the hydroxamic acid and the benzyl residue targeting the S1' pocket were constrained by fixing them. The alignments were performed using the standard parameters and the Amber10:EHT forcefield.

Docking: All dockings were performed with GOLD v5.6.1 in combination with the HERMES visualizer. The docking target meprin β was extracted from the crystal structure (internal communication; PDB ID: 7AQ1). For dockings only chain A and the corresponding zinc ion were used (monomer). For the targets meprin α and ovastacin the recently reported homology models were employed.^[13,14] Compounds **2a**, **2b**, **3a**, **3b**, **4a** and **4b** were docked to a 20 Å radius around the catalytic zinc ion. The hydroxamic acid was substructure constrained, based on the orientation of the co-crystallized hydroxamate of compound 1a. Therefore, a minimum separation (1.5 Å), a maximum separation (3.5 Å) and a spring constant of 5 between the zinc ion and the complexing atoms O4 and O01 of the hydroxamate were defined. All poses were optimized within 10 GA runs and scored with Chemscore[®]. The search efficacy was set to 200%.

Enzymatic assays: Recombinant human meprin β was expressed in yeast and characterized as previously described.^[24] Recombinant human meprin α was expressed and purified from insect cells (S2) and characterized analogously. MMP2, 9, 13, ADAM10 and 17 were purchased from a commercial vendor (R&D systems). MMPs were activated prior to measurement by APMA (*p*-aminophenylmercuric acetate) treatment according to manufacturer's instructions.

The determination of enzymatic activity was based on the cleavage of internally quenched peptide substrates (see supporting information). A typical assay of 250 μ L total volume measured in black 96-well plates consisted of 100 μ L buffer, 50 μ L enzyme at a final concentration of 9×10^{-10} M for meprin α and 3×10^{-10} M for meprin β , 50 μ L substrate (in buffer, 0.05% DMSO) and 50 μ L inhibitor solution (in buffer, 2% DMSO). In case of 125 μ L assay volume (black 96 half area well plates) all volumes were cut in half. Enzymatic activity of ADAMs was measured in 384 well plates with 60 μ L total assay volume consisting of 20 μ L inhibitor or 20 μ L buffer, 20 μ L enzyme and 20 μ L substrate. To ensure reproducibility, the parameters were determined at least in duplicates independently on separate days. For K_i^{app} values the influence of 12 inhibitor concentrations ranging from 2×10^{-4} to 1×10^{-10} M on the enzymatic activity was investigated in the presence of one standard substrate concentration (10 μ M). Initial velocities were determined using a fluorescence plate reader (CLARIOstar, BMG Labtech) at 30 °C. The excitation/emission wavelength was 340/410 nm. The kinetic data was evaluated using GraphPad Prism (version 5.04, GraphPad Software). Kinetic parameters of inhibition (K_i^{app}) were determined using Morrison's equation.^[25]

The inhibitory activity against mouse ovastacin was determined *in vitro* by means of a fluorogenic enzyme activity assay as previously described.^[26] Ovastacin was expressed as previously described^[27] and activated by human plasmin (Haematologic Technologies Inc., Essex Junction, USA) for 30 min in a molar ratio of 10:1. Concentration of active ovastacin (1 nM) was determined

via titration and IC_{50} calculation with heterologously expressed murine fetuin-B^[9]. All assays were performed as independent double measurements in triplicate at 37 °C in 100 μ l final volume, buffered with 150 mM NaCl, 50 mM Tris/HCl, pH 7.4, 0.01% Brij-35. All hydroxamate inhibitors were dissolved in dimethyl sulfoxide. Enzyme activity measurements were started by addition of 25 μ M Ac-R-E(Edans)-D-R-Nle-V-G-D-D-P-Y-K(Dabcyl)-NH₂ ($K_m = 34 \pm 2.2$ μ M), dissolved in dimethyl sulfoxide (final concentration 1.4%). Initial velocities were recorded for at least 1000 s (50 \times 100 ms at intervals of 20 s). Thereafter, 1.5 μ l of proteinase K (at 20 mg/mL; Sigma–Aldrich) were added to reach complete substrate turnover, which was monitored and subsequently calculated using the formula $v = [S] \times m / \Delta F$, where [S] is the substrate concentration, m the $[F/t]$ slope of initial linear substrate turnover, and ΔF the maximal fluorescence intensity corresponding to complete turnover. Kinetic parameters of inhibition (K_i^{app}) were determined using Morrison's equation.^[25]

Cell-viability assay: Cell viability was assessed in human hepatocellular carcinoma cell line Hep-G2 and in human neuroblastoma cell line SH-SY5Y. Hep-G2 cells were cultivated in RPMI1640 (ThermoFisher) supplemented with 10% FBS and SH-SY5Y cells were cultivated in DMEM (high-glucose, pyruvate; ThermoFisher) also supplemented with 10% FBS in a humidified atmosphere of 37 °C and 5% CO₂ (Hep-G2) or 10% (SH-SY5Y) according to standard cell culture procedures. For the assay, cells were plated in 96-well microtiter plates (Greiner bio-one) at densities of 50 000 cells/well (Hep-G2) and 60 000 cells/well (SH-SY5Y). After 24 h, compounds dissolved in DMSO are added to fresh medium without FBS at a concentration of 30 μ M (final concentration of DMSO: 1%, v/v) and applied to the cells for another 24 h. On the next day, cellular viability is determined using the CytoTox-ONE kit (Promega) based on the viability in control wells incubated with culture medium and 1% DMSO. Cells were washed twice with PBS, followed by cell lysis for 10 min (PBS + 9% w/v Triton-X 100). Substrate mix was added and incubated for 10 min in the dark. After stopping the reaction the fluorescence intensity was measured ($\lambda_{ex} = 544$, $\lambda_{em} = 595$ nm).

Acknowledgements

We gratefully acknowledge Antje Hamann and Mercedes Scharfe (IZI-MWT), Dr. Andrea Porzel (Leibniz Institute of Plant Biochemistry, Halle), Dr. Christoph Wiedemann (Martin Luther University, Halle–Wittenberg) and Dr. Christian Ihling (Martin Luther University, Halle–Wittenberg) for their excellent technical support. We also like to thank Dr. Miriam Linnert (IZI-MWT) and Dr. Christoph Parthier (Martin Luther University, Halle–Wittenberg) for providing the crystal structure of meprin β , which will be published elsewhere. Parts of this work were supported by a grant from European Regional Development Fund, #ZS/2019/02/97143 to D.R. Open access funding enabled and organized by Projekt DEAL.

Conflict of Interest

C. J. is employee of Vivoryon Therapeutics N.V., Halle (Saale), Germany. The remaining authors declare no competing interests.

Keywords: heteroaromatics · hydroxamate · meprin · metalloproteinases · ovastacin · scaffold hopping

- [1] F. X. Gomis-Rüth, S. Trillo-Muyo, W. Stöcker, *Biol. Chem.* **2012**, *393*, 1027–104.
- [2] a) E. D. Turtle, W.-B. Ho, *Expert Opin. Ther. Pat.* **2005**, *14*, 1185–1197; b) E. Turtle, N. Chow, C. Yang, S. Sosa, U. Bauer, M. Brenner, D. Solow-Cordero, W.-B. Ho, *Bioorg. Med. Chem. Lett.* **2012**, *22*, 7397–7401; c) M. Talantikite, P. Lécorché, F. Beau, O. Damour, C. Becker-Pauly, W.-B. Ho, V. Dive, S. Vadon-Le Goff, C. Moali, *FEBS Open Bio* **2018**, *8*, 2011–2021.
- [3] a) V. Biasin, M. Wygrecka, L. M. Marsh, C. Becker-Pauly, L. Brcic, B. Ghanim, W. Klepetko, A. Olschewski, G. Kwapiszewska, *Sci. Rep.* **2017**, *7*, 39969; b) C. Broder, P. Arnold, S. Vadon-Le Goff, M. A. Konerding, K. Bahr, S. Muller, C. M. Overall, J. S. Bond, T. Koudelka, A. Tholey, D. J. S. Hulmes, C. Moali, C. Becker-Pauly, *Proc. Natl. Acad. Sci. USA* **2013**, *110*, 14219–14224; c) D. Kronenberg, B. C. Bruns, C. Moali, S. Vadon-Le Goff, E. E. Sterchi, H. Traupe, M. Böhm, D. J. S. Hulmes, W. Stöcker, C. Becker-Pauly, *J. Invest. Dermatol.* **2010**, *130*, 2727–2735; d) J. Prox, P. Arnold, C. Becker-Pauly, *Matrix Biol.* **2015**, *44–46*, 7–13.
- [4] a) T. Bedau, F. Peters, J. Prox, P. Arnold, F. Schmidt, M. Finkernagel, S. Köllmann, R. Wichert, A. Otte, A. Ohler, M. Stirnberg, R. Lucius, T. Koudelka, A. Tholey, V. Biasin, C. U. Pietrzik, G. Kwapiszewska, C. Becker-Pauly, *FASEB J.* **2017**, *31*, 1226–1237; b) O. Breig, M. Yates, V. Neaud, G. Couchy, A. Grigoletto, C. Lucchesi, J. Prox, J. Zucman-Rossi, C. Becker-Pauly, J. Rosenbaum, *Oncotarget* **2017**, *8*, 7839–7851; c) D. Lottaz, C. A. Maurer, A. Noël, S. Blacher, M. Huguenin, A. Nievergelt, V. Niggli, A. Kern, S. Müller, F. Seibold, H. Friess, C. Becker-Pauly, W. Stöcker, E. E. Sterchi, *PLoS One* **2011**, *6*, e26450; d) D. Lottaz, C. A. Maurer, D. Hahn, M. W. Büchler, E. E. Sterchi, *Cancer Res.* **1999**, *59*, 1127–1133; e) P. Minder, E. Bayha, C. Becker-Pauly, E. E. Sterchi, *J. Biol. Chem.* **2012**, *287*, 35201–35211; f) H. Schäffler, W. Li, O. Helm, S. Krüger, C. Böger, F. Peters, C. Röcken, S. Sebens, R. Lucius, C. Becker-Pauly, P. Arnold, *J. Cell Sci.* **2019**, *132*, jcs220665; g) X. Wang, J. Chen, J. Wang, F. Yu, S. Zhao, Y. Zhang, H. Tang, Z. Peng, *BMC Cancer* **2016**, *16*, 383.
- [5] a) S. Carmago, S. V. Shah, P. D. Walker, *Kidney Int.* **2002**, *61*, 959–966; b) C. Herzog, R. Seth, S. V. Shah, G. P. Kaushal, *Kidney Int.* **2007**, *71*, 1009–1018; c) G. P. Kaushal, R. S. Haun, C. Herzog, S. V. Shah, *Am. J. Physiol. Ren. Physiol.* **2013**, *304*, F1150–8; d) B. Oneda, N. Lods, D. Lottaz, C. Becker-Pauly, W. Stöcker, J. Pippin, M. Huguenin, D. Ambort, H.-P. Marti, E. E. Sterchi, *PLoS One* **2008**, *3*, e2278.
- [6] a) S. Banerjee, J. S. Bond, *J. Biol. Chem.* **2008**, *283*, 31371–31377; b) S. Banerjee, G. Jin, S. G. Bradley, G. L. Matters, R. D. Gailey, J. M. Crisman, J. S. Bond, *Am. J. Physiol. Gastrointest. Liver Physiol.* **2011**, *300*, G273–82.
- [7] a) J. Bien, T. Jefferson, M. Causevic, T. Jumpertz, L. Munter, G. Multhaup, S. Weggen, C. Becker-Pauly, C. U. Pietrzik, *J. Biol. Chem.* **2012**, *287*, 33304–33313; b) C. Schönherr, J. Bien, S. Isbert, R. Wichert, J. Prox, H. Altmeppen, S. Kumar, J. Walter, S. F. Lichtenthaler, S. Weggen, M. Glatzel, C. Becker-Pauly, C. U. Pietrzik, *Mol. Neurodegener.* **2016**, *11*, 19; c) C. Becker-Pauly, C. U. Pietrzik, *Front. Mol. Neurosci.* **2017**, *9*, 159.
- [8] a) A. D. Burkart, B. Xiong, B. Baibakov, M. Jiménez-Movilla, J. Dean, *J. Cell Biol.* **2012**, *197*, 37–44; b) H. Körschgen, M. Kuske, K. Karmilin, I. Yiallourou, M. Balbach, J. Floehr, D. Wachten, W. Jahnen-Dechent, W. Stöcker, *Mol. Hum. Reprod.* **2017**, *23*, 607–616; c) W. Stöcker, K. Karmilin, A. Hildebrand, H. Westphal, I. Yiallourou, R. Weiskirchen, E. Dietzel, J. Floehr, W. Jahnen-Dechent, *Biol. Chem.* **2014**, *395*, 1195–1199.
- [9] K. Karmilin, C. Schmitz, M. Kuske, H. Körschgen, M. Olf, K. Meyer, A. Hildebrand, M. Felten, S. Fridrich, I. Yiallourou, C. Becker-Pauly, R. Weiskirchen, W. Jahnen-Dechent, J. Floehr, W. Stöcker, *Sci. Rep.* **2019**, *9*, 546.
- [10] a) E. S. Pires, R. S. D'Souza, M. A. Needham, A. K. Herr, A. A. Jazaeri, H. Li, M. H. Stoler, K. L. Anderson-Knapp, T. Thomas, A. Mandal, A. Gougeon, C. J. Flickinger, D. E. Bruns, B. A. Pollok, J. C. Herr, *Oncotarget* **2015**, *6*, 30194–30211; b) K. A. Knapp, E. S. Pires, S. J. Adair, A. Mandal, A. M. Mills, W. C. Olson, C. L. Slingluff, J. T. Parsons, T. W. Bauer, T. N. Bullock, J. C. Herr, *Oncotarget* **2018**, *9*, 8972–8984.
- [11] D. Ramsbeck, A. Hamann, D. Schlenzig, S. Schilling, M. Buchholz, *Bioorg. Med. Chem. Lett.* **2017**, *27*, 2428–2431.
- [12] D. Ramsbeck, A. Hamann, G. Richter, D. Schlenzig, S. Geissler, V. Nykiel, H. Cynis, S. Schilling, M. Buchholz, *J. Med. Chem.* **2018**, *61*, 4578–4592.
- [13] K. Tan, C. Jäger, D. Schlenzig, S. Schilling, M. Buchholz, D. Ramsbeck, *ChemMedChem* **2018**, *13*, 1619–1624.
- [14] H. Körschgen, C. Jäger, K. Tan, M. Buchholz, W. Stöcker, D. Ramsbeck, *ChemMedChem* **2020**, *15*, 1499–1504.

- [15] L. D. Pennington, D. T. Moustakas, *J. Med. Chem.* **2017**, *60*, 3552–3579.
- [16] W. S. Bechara, I. S. Khazhieva, E. Rodriguez, A. B. Charette, *Org. Lett.* **2015**, *17*, 1184–1187.
- [17] N. Xi, S. Xu, Y. Cheng, A. S. Tasker, R. W. Hungate, P. J. Reider, *Tetrahedron Lett.* **2005**, *46*, 7315–7319.
- [18] Z. Chen, Q. Yan, Z. Liu, Y. Xu, Y. Zhang, *Angew. Chem. Int. Ed.* **2013**, *52*, 13324–13328; *Angew. Chem.* **2013**, *125*, 13566–13570.
- [19] K. Bahrami, M. M. Khodaei, F. Naali, *J. Org. Chem.* **2008**, *73*, 6835–6837.
- [20] S. Mikami, S. Nakamura, T. Ashizawa, I. Nomura, M. Kawasaki, S. Sasaki, H. Oki, H. Kokubo, I. D. Hoffman, H. Zou, N. Uchiyama, K. Nakashima, N. Kamiguchi, H. Imada, N. Suzuki, H. Iwashita, T. Taniguchi, *J. Med. Chem.* **2017**, *60*, 7677–7702.
- [21] D. Yang, D. Fokas, J. Li, L. Yu, C. Baldino, *Synthesis* **2005**, *2005*, 47–56.
- [22] R. P. Kale, M. U. Shaikh, G. R. Jadhav, C. H. Gill, *Tetrahedron Lett.* **2009**, *50*, 1780–1782.
- [23] S. Cai, S. Lin, X. Yi, C. Xi, *J. Org. Chem.* **2017**, *82*, 512–520.
- [24] D. Schlenzig, M. Wermann, D. Ramsbeck, T. Moenke-Wedler, S. Schilling, *Protein Expr. Purif.* **2015**, *116*, 75–81.
- [25] J. F. Morrison, *Biochim. Biophys. Acta* **1969**, *185*, 269–286.
- [26] A. Cuppari, H. Körschgen, D. Fahrenkamp, C. Schmitz, T. Guevara, K. Karmilin, M. Kuske, M. Olf, E. Dietzel, I. Yiallourous, D. de Sanctis, T. Goulas, R. Weiskirchen, W. Jahnen-Dechent, J. Floehr, W. Stoecker, L. Jovine, F. X. Gomis-Rüth, *IUCrJ* **2019**, *6*, 317–330.
- [27] E. Dietzel et al, *Dev. Cell* **2013**, *25*, 106–112.

Manuscript received: October 20, 2020
Version of record online: December 23, 2020